Interfacial Shear Strength of Multilayer Graphene Oxide Films

Matthew Daly,[†,§] Changhong Cao,[‡,§] Hao Sun,[‡] Yu Sun,*[‡] Tobin Filleter,*[‡] and Chandra Veer Singh*[†]

[†]Department of Materials Science and Engineering, University of Toronto, 184 College Street, Toronto, ON, Canada M5S 3E4

[‡]Department of Mechanical and Industrial Engineering, University of Toronto, 5 King's College Road, Toronto, ON, Canada M5S 3G8

S *Supporting Information*

ABSTRACT: Graphene oxide (GO) is considered as one of the most promising layered materials with tunable physical properties and applicability in many important engineering applications. In this work, the interfacial behavior of multilayer GO films was directly investigated via GO-to-GO friction force microscopy, and the interfacial shear strength (ISS) was measured to be 5.3 ± 3.2 MPa. Based on high resolution atomic force microscopy images and the available chemical data, targeted molecular dynamics simulations were performed to evaluate the influence of functional structure, topological defects, and interlayer registry on the shear response of the GO films. Theoretical values for shear

strength ranging from 17 to 132 MPa were predicted for the different structures studied, providing upper bounds for the ISS. Computational results also revealed the atomic origins of the stochastic nature of friction measurements. Specifically, the wide scatter in experimental measurements was attributed to variations in functional structure and topological defects within the sliding volume. The findings of this study provide important insight for understanding the significant differences in strength between monolayer and bulk graphene oxide materials and can be useful for engineering topological structures with tunable mechanical properties.

KEYWORDS: graphene oxide, interfacial shear strength, friction force microscopy, molecular dynamics, shear response, mechanical properties
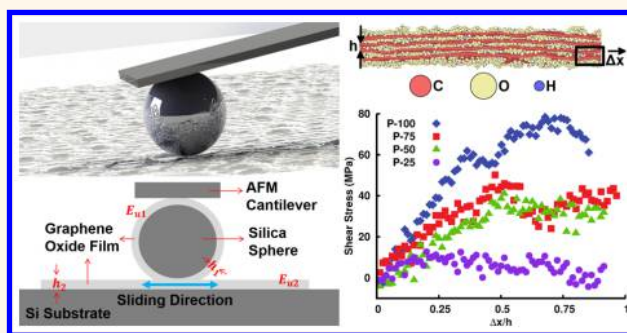
Graphene oxide (GO), as an oxidized form of graphene, has been studied and utilized to form reinforced polymer composites,[1] electrode materials for supercapacitors,[2,3] and transparent conductors.[4] In this role as an important material for next generation energy and lightweight structural applications, the understanding of the mechanical properties of GO is of significant interest. Recent experimental measurements have shown that the strength of monolayer GO is in the range of 20−30 GPa.[5] However, GO in paper form (micrometers thick) exhibits a strength of ~100 MPa.[6] This significant size-induced difference in mechanical strength can be attributed to higher void densities between layers in thicker films[7,8] and a transition in the failure mechanism, from in-plane fracture toward interplanar failure.[7,9] This transition in the fracture mechanism is governed by shear between adjacent layers in multilayer GO films. A similar size effect in structure−property relationships has been reported for other carbonaceous materials such as carbon nanotubes (CNTs). Individual CNTs possess extraordinarily high mechanical strength on the order of ~100 GPa.[10] However, in bulk CNT fibers,[11] the domination of weak van der Waals interactions between

individual constituents[12] leads to reductions in mechanical properties by orders of magnitude.[11]

The interfacial shear strength (ISS), which is the stress required to cause sliding between adjacent layers, is considered to be a critical parameter in defining the transition between monolayer and bulk strengths in multilayer GO films as it governs the mechanics of load transfer between adjacent layers. Despite its significance, experimental measurement of the ISS of multilayer GO has not been reported. Previous investigations have measured the ISS for other carbonaceous nanomaterials such as graphene,[13] and multiwalled CNTs[12,14−16] and have indicated that interlayer friction is fundamentally stochastic in nature.[17] For example, shear strengths of multiwalled CNTs have been reported to vary in the range of 0.05−4.0 MPa.[12,14−16] Similarly, graphite is reported to have a ISS in the range of 0.25−2.5 MPa.[13,18] Furthermore, the interfacial behavior in GO films is intricately linked to the nature of

functional groups and the presence of topological defects. A fundamental understanding of the interfacial behavior and measurement of ISS is thus essential to accurately predicting and interpreting the ultimate strength of multilayered GO films, providing mesoscale insight which can be leveraged toward engineered bulk materials with tailored mechanical properties.

While a direct experimental measurement of the ISS of multilayer GO is currently absent in the literature, theoretical calculations enabled by density functional theory (DFT) have estimated the ISS of GO interfaces to be between 0.33 GPa (graphene) and 4.48 GPa for GO samples of various oxidation levels.[19] However, the applicability of these results remains limited due to the inherent limitations of DFT analysis such as simulation cell size restrictions and the omission of kinetic factors including temperature and sliding rate effects. On the nanoscopic scale, the ISS of multilayer GO is a manifestation of interatomic interactions between different functional groups (*e.g.*, hydroxyl and epoxide[20,21]) which populate graphene monolayers. The 10-fold increase in ISS between graphene and GO predicted by Wang *et al.*[19] highlights the critical role that material chemistry and functional structure hold in determining physical properties. Molecular dynamics (MD) simulations have been utilized to examine larger-scale functional effects such as the influence of water content and interlayer hydrogen bonding on in-plane stiffening under uniaxial tensile[22] and layer pullout conditions.[23] Due to the heterogeneous nature of layering in bulk GO materials,[7,8] topological defects are also expected to strongly influence the ISS of multilayer GO. For example, in a DFT study of topological defects, Paci *et al.*[24] showed a decrease of approximately 37% in the in-plane strength of monolayer GO due to the presence of an atomic scale hole, highlighting the impact of topological defects on the mechanical response of planar structures. Nonetheless, the influence of functional and topological structure on the ISS of GO has not been reported in the literature.

In the present work, a combined experimental-computational approach is utilized to investigate the ISS of multilayer GO. Tribological studies via friction force microscopy (FFM) testing were performed to experimentally determine the ISS of GO interfaces. MD simulations of interlayer sliding in multilayer GO were utilized to investigate the effects of chemistry and topological defects on the ISS. Additionally, the influence of interplanar registry is also examined, as incommensurate interlayer contact has been shown to strongly influence the ISS of multilayer graphene.[25,26] These simulations permit atomic-scale observation of the shearing process and provide physical insight into the influence of topological variations on the ISS, as well as contextualize the scatter measured in the experimental data. The results of this study are expected to be critical to the design of GO-based materials and are necessary to understand the order of magnitude differences between monolayer and bulk GO mechanical properties.

RESULTS AND DISCUSSION

Characterization of Deposited GO Films. FFM with a modified atomic force microscopy (AFM) probe was applied to measure the ISS of GO layered films. Instead of using the standard sharp Si AFM probes, a GO-coated silica spherical tip was utilized to directly perform sliding tests on a GO-coated Si substrate such that the interfacial property between the two GO surfaces was measured. The GO flakes (Cheap Tubes Inc.) were synthesized using the modified Hummer's method.[27] Raman spectroscopy was performed and reported elsewhere[5] to

reveal the D (1345 cm^{-1}) and G (1598 cm^{-1}) peaks, which are characteristic of the GO structure.[28] We conducted X-ray photoelectron spectroscopy (XPS) analysis that measured the carbon-to-oxygen ratio of the tested samples to be approximately 4:1 and identified the relative structural compositions of sp^2/sp^3 carbon (67.1%), hydroxyl/epoxide surface groups (22.1%), and edge groups (10.8%).[29] Due to very similar binding energies, it is challenging to uniquely determine a specific quantification of hydroxyl and epoxide groups, and therefore, the hydroxyl/epoxide XPS peak was not deconvoluted. The preparation of the GO-water solution used for coating the substrate and AFM probe surfaces with GO is further discussed in the Methods section and is also reported elsewhere.[5] Before ISS measurement, the deposited GO films were examined using sharp AFM Si probes, and three major defect types, island, fragment, and hole, were identified under high resolution AFM topography images (see the Supporting Information). Similar defects were also observed in our previous work.[29] Figure 1 shows a schematic of the
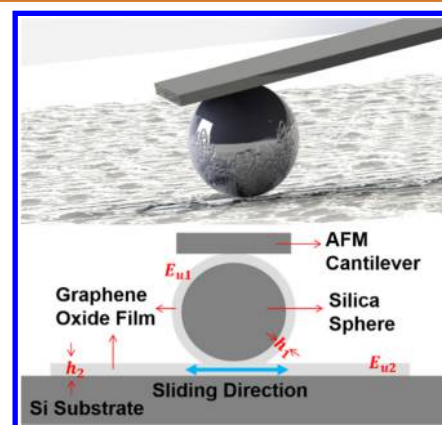

Figure 1. Schematic illustrating the experimental setup (not drawn to scale). The AFM cantilever with a silica spherical tip coated with GO film (coating thickness, h_1; reduced modulus, E_{u1}) was laterally dragged across the GO deposited (thickness, h_2; reduced modulus, E_{u2}) Si substrate. See the Supporting Information for a further description of these parameters and their usage.

experimental setup. The AFM cantilever used for ISS measurement was fabricated by adhering a silica sphere with epoxy (∼30 μm in diameter) to a standard silicon cantilever, providing a quasi-planar contact area as compared to the sharp point of a standard AFM tip.

As GO film thickness is known to be proportional to the concentration of GO solution,[30] a 10 mg/mL GO concentration was used, which correlates to a film thickness of ∼60 nm. This thickness was confirmed via AFM topography scanning of a GO film which was deposited through drop casting from the same solution onto a Si substrate. Scanning electron microscopy (SEM) images and energy-dispersive X-ray spectroscopy (EDX) carbon maps were collected on the spherical bead before and after GO film coating, as shown in Figure 2. Before GO coating, the major carbon sources were the adhesives used to attach the silica sphere to the AFM cantilever. No obvious carbon signal was collected from the sphere itself (Figure 2a and c). After coating, SEM images clearly showed that the silica sphere was covered with GO films (Figure 2b). EDX carbon mapping further confirmed the presence of a significant amount of carbon on the spherical tip (Figure 2d). Please note that the spherical tips imaged in Figure
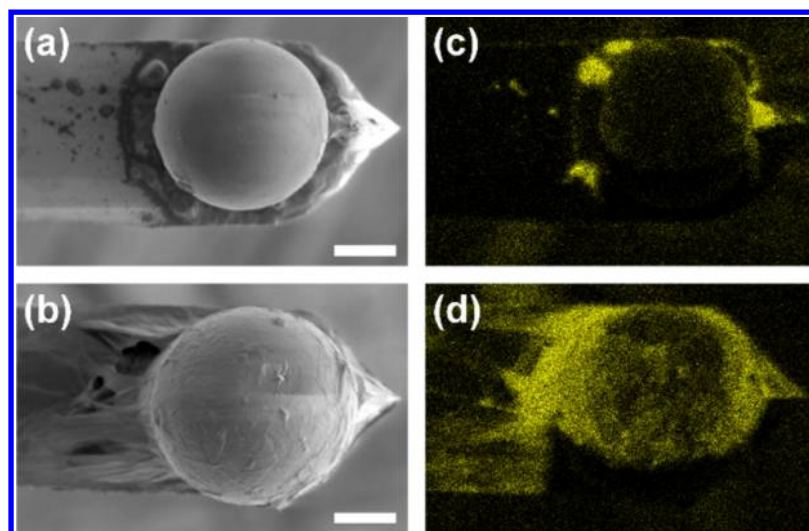
Figure 2. SEM images of the AFM cantilever before (a) and after (b) GO film coating (scale bar: 10 μm). (c, d) EDX carbon maps of the cantilever shown in (a) and (b), respectively.

2 are not the same AFM probes, but rather represent typical tip conditions with and without GO coatings.

Experimental ISS Measurements of GO Film Interfaces. In order to measure the ISS between GO films, the AFM cantilever with a GO-coated spherical tip was brought into contact with the GO-covered Si substrate. A SEM image of the as-deposited GO on the Si substrate and an AFM topography scan of the film (using the GO-coated silica spherical tip) are provided in Figure 3a and b, respectively. Contact AFM operated in a friction force microscopy mode was conducted by sliding the tip relative to the sample in the direction perpendicular to the cantilever long axis at a scan rate of 2.5
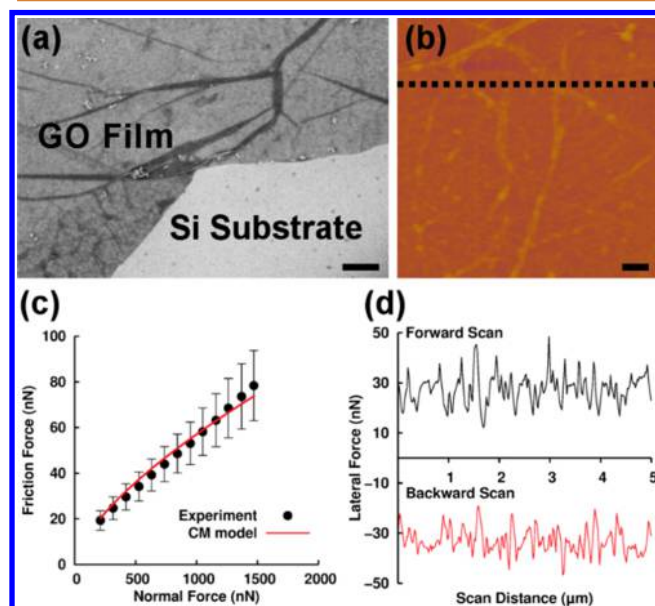

Figure 3. (a) SEM image of the as-deposited GO film on the Si substrate (scale bar: 500 nm). (b) AFM topographical image of a GO film scanned by the GO coated silica sphere (scale bar: 500 nm). (c) Representative plot of friction force vs normal force and a Maugis−Dugdale fit (see details in the Supporting Information). (d) Lateral force of forward and backward scan at a 500 nN normal load along the dashed line in (b).

μm/s, as illustrated in Figure 1. Prior to attaching the silica sphere to the AFM cantilever, the normal and torsional spring constants were calibrated. After attaching the silica sphere (but prior to GO deposition), the normal and lateral sensitivity of the AFM was calibrated (see Methods section). Figure 3c shows a representative plot of normal force vs friction force recorded during sliding between the two GO surfaces. The data was fit to a Maugis−Dugdale[31] contact mechanics (CM) model (see the Supporting Information). For each data point (with a fixed normal load), 256 scan lines were performed in a 5 μm × 5 μm area, and the friction force was determined from the forward and backward scans of the friction loop and averaged over all scan lines. The normal load was increased from 200 to 1500 nN with an increment of 100 nN to obtain the relationship between normal force and friction force. In this loading range, wear was not observed on the GO surface. Figure 3d presents the lateral force of forward and backward scans at ∼500 nN normal load along the dashed line in Figure 3b. For normal loads higher than 1500 nN, wear of the surface was evident from subsequent AFM imaging. Therefore, friction measurements collected up to a normal load of 1500 nN were considered to be within the wear-free regime.

Ten independent ISS measurements were conducted, and the normal load vs friction force data (Figure 3c) on different testing sites of the deposited GO film were analyzed following the method of Carpick et al.[32] (see the Supporting Information). Measurement of the ISS ranged from 2.3 to 11.6 MPa with an average ISS of 5.3 ± 3.2 MPa. Error is reported here in terms of the standard deviation ($n = 10$). The large scatter in ISS measurements may be attributed to sample variations as a different scanning region was chosen for each measurement. Heterogeneous surface features were observed in the SEM image of the coated sphere and substrate which may indicate the presence of topological defects, film wrinkling, and heterogeneous stacking in the film cross-section. In this context, each experimental measurement homogenizes a convolution of structural factors such as local variations in topological defect density and functional group distribution within the contact regions. Taken together, these factors contribute to the measured variations in the ISS values. The influences of each of these topological variations may not be directly probed

experimentally; however, MD simulations were implemented to assess their potential individual impact on the ISS and are discussed in the next section.

Theoretical ISS Determination via MD Simulations. In order to provide an upper bound estimate for the ISS, as well as assess the influence of functional and topological structure on the shear response, targeted MD simulations were performed. GO films were constructed based on the available XPS measurements.[29] Each MD supercell possessed lateral dimensions measuring at least 175 Å by 150 Å in the zigzag and armchair directions, respectively, and was composed of at least four GO layers through the thickness (~28 Å thick). Fixed boundary conditions were enforced in all dimensions during shear loading. Edge groups (*i.e.*, carbonyl and carboxyl) were not considered in this study, as they are likely only attached to edge atoms with dangling bonds and atoms possessing this local environment represented ~2−3% of all atoms in the supercell. Upon elimination of edge groups from spectroscopy data, a carbon-to-oxygen of approximately 5:1 was assumed for the surface functional groups. Given the notable influence of the hydroxyl/epoxide groups on ISS,[19] and the relative uncertainty of the exact distribution of planar functional groups in GO, MD simulations with an assumed 25%, 50%, 75% and 100% hydroxyl group distribution were performed, with the balance of functional groups being designated as epoxide structures. For example, a 75% hydroxyl functionalization refers to a structure whereby the total number of oxygen atoms are determined by the 5:1 carbon-to-oxygen ratio, and the distribution of these oxygen atoms into hydroxyl and epoxide function groups occurs at fractions of 75% and 25%, respectively. Figure 4a illustrates a GO film cross section possessing both hydroxyl and epoxide structures with an equal functional (50%) distribution. The condition of 0% hydroxyl was found to be unstable in MD simulations, which is consistent with previous DFT studies of purely epoxide GO.[33]

In addition to functional structural considerations, topological defects are also anticipated to influence the mechanical properties. The heterogeneous layering of GO films in hierarchical paper structures presents a number of topological defects which may be considered for study[7,8] While a plethora of unique topologies are possible in multilayer GO, MD simulations were designed to individually target defect structures whose signature was identifiable in AFM topographic scans of the as-deposited GO films (see the Supporting Information). Specifically, planar fragments of GO layers ("fragment"), large holes in the sample cross section ("hole"), and isolated intercalated GO flakes ("island") were investigated in MD simulations. Figure 4b provides a schematic of the topological defects examined in this study. In order to simplify the representation of different models, short-hand notations are used to represent the island (I), fragment (F), and hole (H) topological defects. Structures without topological defects are considered to be in a quasi-pristine (P) condition. Differences in functional structure are represented as percentages and are appended to the appropriate topological symbol. For instance, H-100 indicates a hole defect with a 100% hydroxyl functionalization. Shear deformation of the GO interface is achieved by relative sliding of layers in the zigzag direction, as shown in Figure 4c. As indicated in the figure, the abscissa is measured here as the ratio of sliding displacement (Δx) over the interlayer spacing (h). For the purposes of normalized displacement calculations, a constant interlayer spacing value of 7 Å was assumed, which is consistent with previous studies.[5,34]
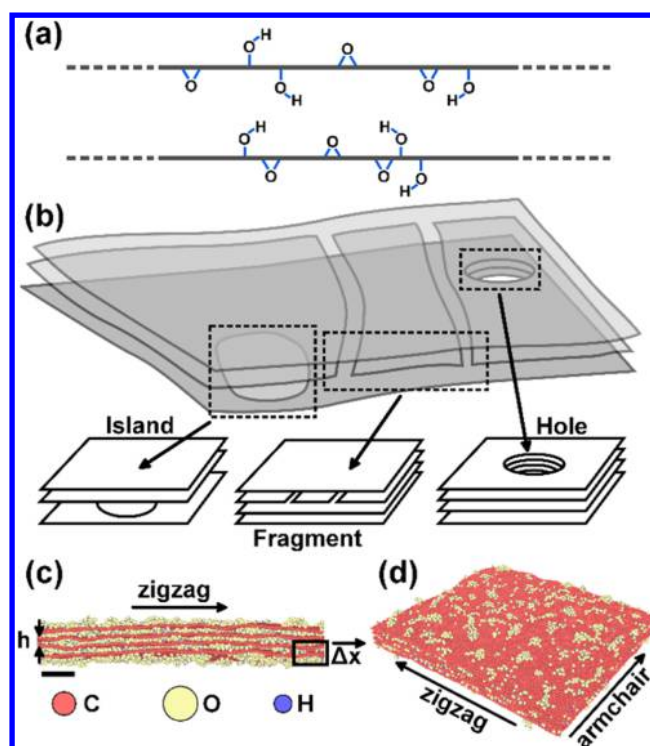

Figure 4. (a) Cross section schematic showing the configuration of hydroxyl and epoxide functional groups attached to the carbon planes in GO films. (b) Schematic of a GO film composed of island, fragment, and hole topological defects. Schematics of their initial structures in the MD supercell are indicated by the arrows. The atomic representations of these topological defects are provided in the Supporting Information. The relaxed P-100 topology in cross section (c) and perspective (d) views. Undulations in the graphene plane as well as agglomerations of functional groups are clearly visible. Sliding between GO layers is directed as indicated by the arrow in the figure. The displacement (Δx) is normalized against the assumed interlayer spacing (h = 7 Å). The principal directions of the graphene planes are indicated in the figure, and shearing is performed in the zigzag direction. The scale bar in (c) corresponds to 2 nm.

As shown in Figure 4c and d, during relaxation, the functional groups were observed to coalesce into larger agglomerates, which is consistent with previous studies[9] and transmission electron microscopy investigations of GO monolayers.[35] These agglomerates connect adjacent GO layers via hydrogen bond networks and serve as the primary stiffening agent in the shear response of the GO films. It should be noted that, although localized Ångstrom-scale undulations exist in the topology, the GO films are nominally flat in MD simulations, whereas in the experimental study the GO layers are fixed to the surface of a sphere. However, given the orders of magnitude difference between the length-scales of the spherical tip radius and the MD simulation cell, a flat contact area may be reasonably assumed on the atomistic scale. Specifically, the 30 μm spherical AFM tip subtends an angle of less than 0.07° along the MD supercell lateral dimensions (175 by 150 Å).

The process of interfacial sliding is illustrated at different snapshots of deformation in Figure 5. From an atomistic perspective, interlayer slip initiates when hydrogen bonds in the gallery space begin to break. Under continuous slip, these bonds are continually broken and reformed at a quasi-isostress condition and reduced load (*i.e.*, static *vs* dynamic friction).
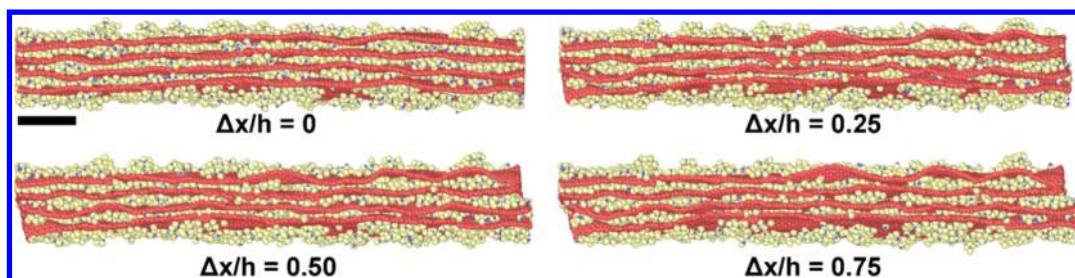
Figure 5. Snapshots of sliding deformation in the P-100 hydroxyl sample. Relative sliding of the layers is evident at higher $\Delta x/h$ ratios. Scale bar corresponds to 2 nm.

This mechanical response is qualitatively observed in the collected MD data. However, due to the large loading rates associated with MD simulations, it is not possible to directly observe a perfect static-dynamic transition in the shear loading curve. The ISS was defined as the maximum shear stress value using the Virial stress formulation in the MD simulations of GO film sliding. The collected shear stress data points were averaged over a time frame of 1 ps, which corresponded to the relaxation time between the incremental displacements of sliding layers.

Effect of Functional Structure on ISS. As shown in Figure 6a, the P-100 structure, comprised of entirely hydroxyl groups, possessed the highest ISS (78 MPa) of all the topologies
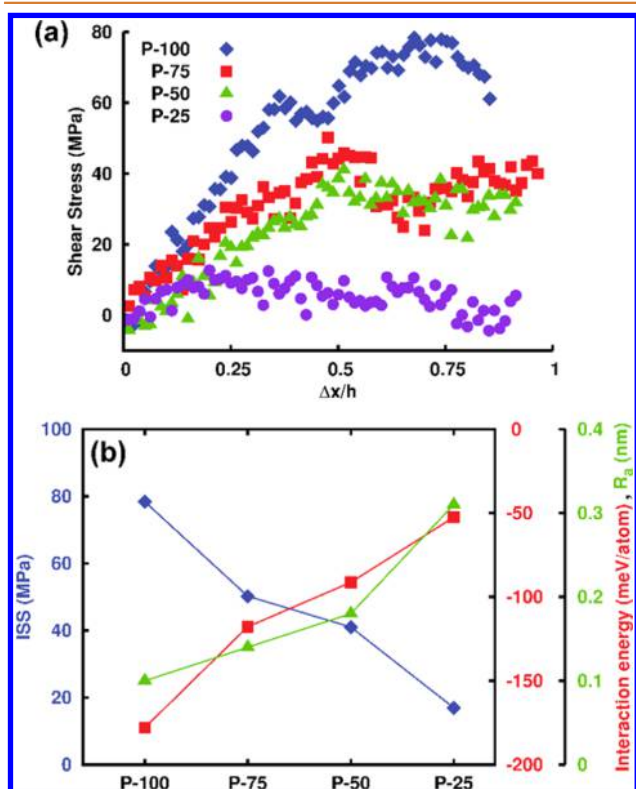

Figure 6. (a) Shear response of GO samples with varied functional structure. Within the context of functional structure, P-100 data denotes a structure without topological defects which possesses a 100% hydroxyl functional distribution. Similarly, P-75, P-50, and P-25, denote structures with 75%, 50%, and 25% hydroxyl functionalities, respectively, with the balance of structures being epoxide groups. (b) Normalized interaction energy and layer roughness are found to increase monotonically with respect to epoxide content, which leads to a corresponding decrease in ISS.

considered in this loading configuration. This value was found to be insensitive to the applied shear displacement rate (see the Supporting Information). In comparison to existing DFT measurements (*e.g.*, 4.48 GPa[19]), the present MD simulations provide a prediction that is much more consistent with the experimental data. The discrepancy between DFT and MD predictions highlights the need to consider both thermal effects, as well as factors such as surface roughness, which cannot be captured within the framework of comparatively small-scale athermal DFT simulations. It should be noted that while every effort was made to relax topologies prior to loading, small residual stresses (on the order of ±5 MPa) were unavoidable due to limitations on the simulation cell size. Specifically, the presence of unbalanced short-range undulations in the graphene plane, as well as complex stress fields around defects are expected to have an exaggerated impact on the global stress-state, leading to the observed measurement error.

Introduction of epoxide groups was found to drastically reduce the ISS of the GO films monotonically from 78 MPa (P-100) to 17 MPa (P-25). Additionally, the changes in chemistry had a significant impact on the stiffening of the shear response (*i.e.*, on the slope of stress-displacement curve). As shown in Figure 6b, the normalized interaction energy of hydrogen bonding in the GO preparations was found to monotonically increase with epoxide content. The normalized interaction energy was defined as the time-average of the total sum of hydrogen bonding interactions in the supercell during the last picosecond of topology relaxation divided by the number of functional atoms (*i.e.*, oxygen and hydrogen). In the context of interaction energies, lower values represent increased bonding. Since the interfacial distances are almost identical between samples (see the Supporting Information), the decrease in ISS can be attributed to a drop in the density of hydrogen bonds within the GO structure when hydroxyl groups are replaced with epoxide structures, leading to reduced stiffness and lower shear strengths. Furthermore, an increase in roughness (R_a) was observed at a lower hydroxyl functionalization, consequently reducing the effective contact area between sheets (Figure 6b). It is not clear from the current data as to the correlation between functional structure and the amount of slip required to achieve maximum shear stress. However, similar shifts in the position of stress–strain inflection points have been observed in other MD studies of layer pullout in GO films.[23]

Effect of Topological Defects on ISS. In addition to chemical structure effects, topological defects were also found to influence the ISS of GO films. As shown in Figure 7a, the ISS of the F-100, H-100, and I-100 structures were determined to be 71, 52, and 26 MPa, respectively. The island model corresponds to a decrease of 67% in ISS when compared to the P-100 reference (78 MPa). The ISS of GO films therefore was
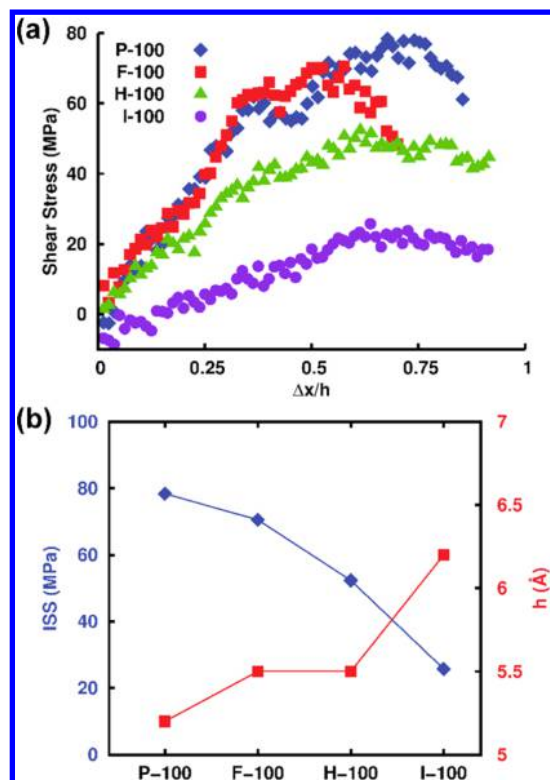
Figure 7. (a) Shear response of GO samples with different topological defects. The label P-100 corresponds to a structure without a defect, whereas the labels F-100, H-100, and I-100 denote topologies with a fragment, hole, or island defect, respectively. (b) Collected ISS measurements plotted alongside the average interlayer spacing. A decrease in the ISS may be clearly linked to a substantial increase in the interlayer spacing of the I-100 sample.

found to be sensitive to the insertion of GO flakes in the gallery space. With respect to shear loadings, the insertion of a GO flake increased the local interlayer spacing as the surrounding layers conformed to the intercalated plane. Indeed, the average interlayer spacing of the island structure was estimated to be 6.2 Å, which is approximately 13−19% larger than the interlayer spacing estimated for the hole (5.5 Å), fragment (5.5 Å), and P-100 (5.2 Å) structures (Figure 7b). From a geometric perspective, the localized increase in interlayer spacing reduces the interactions of intercalated functional groups, and subsequently reduces frictional forces. Contrary to the island topological defect structure, both the hole and fragment models were not observed to cause a drastic reduction in ISS. The slight decrease of ISS was attributed to the lesser number of atoms under shear deformation. In uniaxial tension studies, these void-type defects are often strength-defining as they reduce the effective load-bearing cross-section of the structure. However, under shear loading of a planar structure such as GO, failure does not proceed from a weakest-link member (i.e., stress concentration). Rather, the removal of material reduces the total frictional force that the GO flakes may exert as they slip past each other under shear loading, which leads to only a moderate decrease in ISS.

Influence of Interlayer Registry on ISS. Beyond chemical and topological defect factors, poor interlayer registry and incommensurate contact is known to cause a significant variation in friction and subsequently a several order of magnitude decrease in the ISS of multilayer graphene.[25,26] The effect of interlayer registry was therefore studied by rotating the

sliding layers of the P-100 preparation through an angle (θ) and then performing a shearing simulation using the same approach previously implemented. Due to periodicity requirements during supercell relaxation, specific angles corresponding to coincident site lattice rotations were selected for study. Namely, supercells possessing rotations of 9.4, 21.8, 27.8, 32.2, 38.2, and 50.6° were created for shearing simulations. A detailed description of the construction procedure may be found in Carlsson et al.[36] In addition to a study of the effects of registry, shearing in the armchair direction of the P-100 structure was also investigated. Figure 8a provides a schematic illustration of
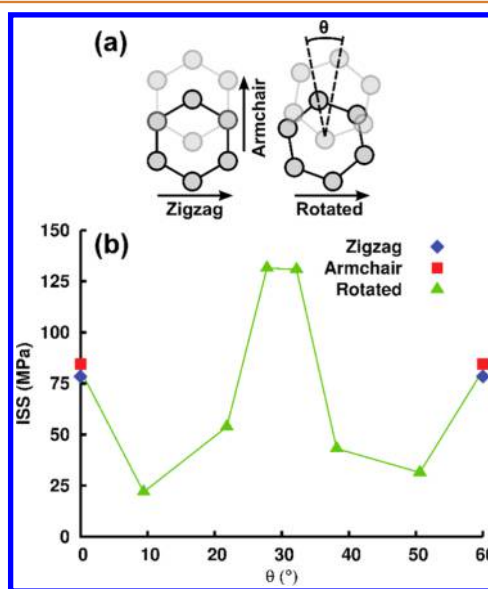

Figure 8. (a) Schematic showing the structural orientation for carbon atoms under armchair and zigzag shearing as well as systems with rotated sliding layers. Translucent atoms are in a layer above the opaque atoms. (b) Collected ISS measurements of the rotated P-100 sample illustrating a mirror symmetry at an angle of 30°.

the rotated topological configuration as well as the sliding directions for zigzag and armchair shearing simulations. The armchair and zigzag shear simulations were found to result in very similar ISS values of 84 and 78 MPa, respectively. As shown in Figure 8b, with respect to the influence of interlayer registry, incommensurate contact showed a more pronounced effect with ISS data ranging from 22 (~10° rotation) to 132 MPa (~30° rotation). The ISS values for the rotated system also appear to exhibit mirror symmetry at a 30° rotation angle. This observation is in contrast to the 60° symmetry reported by Dienwiebel et al.[26] However, this result is consistent within the context of interlayer registry symmetry and consideration of the near congruence between the zigzag and armchair ISS measurements (i.e., as constructed here, a 10° and 50° sliding tests are geometrically analogous to zigzag and armchair shearing of the nonrotated structure). The overall influence of registry results in an approximate 2−3-fold change in the ISS of GO films. Notably, this change is less significant when compared to the 3−4 order of magnitude change reported for "lock-in" states in graphene.[25] In comparison to graphene, the muted influence of registry is anticipated in the GO structure as the shear response is dominated by intercalated functional groups which create corrugations within the topology and increase the interlayer spacing of layers. In this

Table 1. Theoretical Predictions and Experimental ISS Measurements of GO Interfaces

theoretical predictions						experimental measurements	
functional structure variation		topological defect variation		interlayer registry variation		FFM measurements	
% hydroxyl	ISS (MPa)	structure	ISS (MPa)	rotation (deg)	ISS (MPa)	ISS (MPa)	
100	78	pristine	78	0 (zigzag)	78	5.3 ± 3.2	
75	50	fragment	71	0 (armchair)	84		
50	41	hole	52	9.4	22		
25	17	island	26	21.8	54		
				27.8	132		
				32.2	131		
				38.2	43		
				50.6	31		

context, the undulated structure of GO limits the influence of atomic registry between carbon planes on the ISS. Indeed, observation of the highest ISS at orientations rotated from the nominal ABAB stacking configuration underscores the absence of a direct link between registry and ISS.

Comparison between MD Simulations and Experiments. The ISS of the GO films was experimentally measured to be 5.3 ± 3.2 MPa, which is approximately twice as large as upper bound values reported for bulk graphite (2.5 MPa).[18] The presence of functional groups in the gallery space of GO leads to better interlayer adhesion via hydrogen bonding and is responsible for its relatively higher ISS. This measurement is particularly consequential, as it highlights the large strength difference between intraplanar fracture (GPa range) and interplanar shearing (MPa range) failure modes. In this regard, the ISS of GO serves to explain the drastic drop in the mechanical strength of monolayer GO (intralayer failure) when compared against bulk GO (interlayer failure). Individual experimental measurements of ISS were found to vary from 2.3 to 11.6 MPa. In comparison, when functional structure, topological defects, and interlayer registry were considered, MD simulations revealed strengths as low as 17 MPa, showing good agreement with experimental measurements and providing realistic upper bounds for ISS measurements in GO films (see Table 1). Furthermore, MD results showed the significant impact of both the character of functionalization as well as the presence of topological defects. The quasi-pristine GO system (*i.e.*, devoid of topological defects) showed an ISS of up to 132 MPa (100% hydroxyl functionalization), indicating that with careful control of GO film structure, the ISS can be significantly improved. The explicit differences between MD and experimental measurements may be rationalized by considering the different scales of roughness which influence the effective contact areas in each approach (see the Supporting Information). Additionally, experiments represent a largely dynamic measurement (averaged frictional force during AFM line scan), whereas MD simulations assess the static friction to sliding (maximum stress), which also may lead to some overestimation of the ISS. Notably, the ISS strengths computed at an order of magnitude lower applied shear displacement rate in MD simulations did not result in a statistically significant change in values, suggesting that shear behavior in multilayer GO may be loading rate independent (see the Supporting Information).

In addition to providing upper bound estimates of ISS, the MD simulations provide insight when considering the scatter in the experimental data sets. By taking the ratio of the standard deviation to its average, the coefficient of variation (CV) may be obtained, which may be used as a metric to examine the degree of variability in each measurement. Under this definition, CVs of 0.6 and 0.52 are calculated for experimental and MD data sets. Therefore, while the absolute values of ISS may not be directly compared, the calculated CVs indicate a similar degree of variability in each measurement set. In this regard, the scatter in experimental results can be interpreted as a difference in topological configuration between individual ISS measurements and MD simulations provide a targeted assessment of each structural variation. Furthermore, MD results show that the degree of hydroxyl functionalization, orientation of sliding layers, as well as the presence of small intercalated flakes cause the largest drops in ISS. Other topological defects such as planar flake fragments or large through-holes are not predicted to have a large impact on ISS. Uniformity in the size distribution and functional structure of deposited GO flakes are therefore implicated as the critical parameters in establishing strong interlayer bonding in GO films.

CONCLUSIONS

The ISS of GO films were experimentally measured using FFM to be 5.3 ± 3.2 MPa, which is at least two times greater than that of graphite. This comparative increase is attributed to stronger interlayer bonding due to the presence of intercalated functional groups. Targeted MD simulations were performed to provide realistic upper bound estimates of ISS and to study the influence of functional and topological structure on the ISS of GO. MD results predict an ISS as low as 17 MPa, which is very close to experimentally measured values and in much better agreement than existing DFT estimates. From MD simulations, ISS measurements were found to be very sensitive to the degree of hydroxyl functionalization, the presence of isolated intercalated flakes, and the orientation of sliding layers. At lower levels of functionalization, the ISS was found to decrease significantly, which was attributed to a decrease in hydrogen bonding and an increase in the surface roughness. Additionally, the presence of intercalated flakes was found to increase interlayer spacing, subsequently lowering the ISS. The orientation of sliding layers was also found to have an effect on the ISS. However, this influence was found to be less significant than previously reported strength variations arising from incommensurate surface registry in multilayer graphene. The MD results also revealed the atomic origins of the large degree of scatter in experimental measurements. A comparison of coefficients of variation between experimental and MD data sets indicated that the stochasticity in ISS may be attributed to the differing chemical and topological structures, as well as the registry of sliding surfaces, which are inherently varied in

experimental measurements. These findings provide mesoscale structure—property insight which can be leveraged toward engineered bulk materials with tailored mechanical properties.

METHODS

Experimental Methodology. Silica spheres (Polysciences Inc.) were glued to AFM cantilevers with epoxy using a custom-built micromanipulation stage coupled with an optical microscope. A GO solution was synthesized by slow-stirring GO flakes (Cheap Tubes Inc.) in water for 2 weeks, and centrifuging (Cole-Parmer) the solution at 3000 rpm to remove unexfoliated GO flakes and then at 5000 rpm to obtain a precipitate containing only large GO flakes. The resulting GO solution was then drop-cast on the surface of a silicon substrate as well as on top of a silica sphere (~30 μm in diameter) attached to an AFM cantilever. The dropcast samples were then dried at 80 °C to ensure a uniform coating on both the sphere and substrate. AFM imaging using the spherical probe was recorded using an Asylum MFP 3D instrument. SEM imaging and EDX analysis were performed using a Hitachi SU3500 electron microscope equipped with an Oxford Instruments X-max detector (127 eV resolution at 5.9 keV). SEM imaging of the sphere was completed under a 1 kV acceleration voltage, and EDX measurements were collected by increasing the gun voltage to 5 kV to excite a broader band of X-rays but remain relatively surface sensitive. High resolution SEM imaging of the GO film deposited on Si substrate was conducted under a 1 kV acceleration voltage using a Hitachi SU 4800 instrument. Sliding tests under AFM were performed in friction force microscopy (FFM) mode with a 90° scan angle and a scan rate of 2.5 μm/s. The lateral sensitivity of the AFM was calibrated by horizontally pushing the silica sphere against the side wall of a freshly cleaved KBr to acquire the electrical signal of lateral deflection response versus lateral displacement of the cantilever.[37] Normal sensitivity of the AFM was measured by recording a normal deflection vs displacement curve on a rigid Si substrate to extract the signal of normal deflection response versus cantilever displacement in the normal direction. Normal and torsional spring constants were calibrated using Sader's method[38] before attaching the silica sphere to be 1.25 N/m and 2.14 × 10⁻⁸ N·m/rad, respectively. AFM contact mode with a sharp Si probe was utilized to obtain topographical images of the GO defect structures.

Molecular Dynamics Simulations. The Large-scale Atomic/Molecular Massively Parallel Simulator (LAMMPS)[39] was used to perform MD simulations with interatomic interactions modeled by the ReaxFF potential.[40] ReaxFF is a bond-order-based potential which is capable of capturing the bonded and nonbonded interactions between different atoms in the graphene oxide system. It has been implemented in a number of previous nanomechanical studies of the GO system.[9,22,23] The nearest neighbor and hydrogen bond cutoff radii were set to 5 and 7.5 Å, respectively. As reported previously, the interaction energy of hydrogen bonds approaches zero at distances of above 6 Å.[22] The simulation cell measured approximately 175 by 150 Å in the lateral dimensions respectively, and each simulation cell possessed a minimum of four layers through the cross section (~28 Å thick). The initial positions of epoxide and hydroxyl groups were assigned as per the Lerf−Klinowski model,[20] whereby sites for epoxide and hydroxyl binding were selected at random, with equal probabilities of selection being assigned to binding sites above and below graphene planes. Upon initialization of the MD model, the initial interlayer spacing was set to 7 Å, which is the effective layer thickness commonly assumed in studies of GO films.[5,34] Following knowledge gained from previous electron diffraction studies of basal plane stacking in bulk GO,[41] an ABAB stacking for GO layers was utilized to create the model. Prior to shear loading, the system was heated to the target temperature (300 K) using the Nosé-Hoover thermostat over a period of 25 ps. The GO sample was then equilibrated at this temperature to minimize the system pressure and allow for cell relaxation. Heating and equilibration routines were performed under periodic boundary conditions along the lateral dimensions of the GO layers and a fixed boundary condition in the out-of-plane direction. These boundary conditions were selected to eliminate large undulations associated with free planar edges. During shear loading of the unit cell, the boundary conditions were reassigned to be fixed in all three directions. In order to best approximate experimental loading procedure, the top two GO layers were displaced at a constant rate by dilating the simulation cell along the shearing direction and simultaneously performing an equal affine transformation to atom positions in the displaced layers (LAMMPS; *fix deform* command). Atoms in ~20 Å strips on opposing edges of the simulation cell were frozen to prevent rigid-body translation or unloading of the GO structure. Sliding operations were performed such that only atoms in the frozen region were directly displaced. Movement in the remainder of the supercell, including the intercalated functional groups, was directed purely by the system dynamics. The effective average displacement of carbon atoms in the displaced layers was ~0.1 Å/ps. In consideration of system size effects, the number of layers displaced during shearing and the total number of layers within the supercell were also varied to assess their influence on the ISS (see the Supporting Information). Stress was calculated using the Virial theorem, and a time step of 0.25 fs was utilized in all MD simulations. The Open Visualization Tool (Ovito)[42] was used to visualize atomic topologies.

ASSOCIATED CONTENT

⑤ Supporting Information

The Supporting Information is available free of charge on the ACS Publications website at DOI: 10.1021/acsnano.5b05771.

Atomic force microscopy topographical imaging of defect structures; experimental mechanics model for interfacial shear strength of GO; atomic topologies of defect structures; surface roughness and interfacial distance; effect of sliding rate on ISS; influence of the number of displaced layers and number of layers in the MD supercell on the ISS (PDF)

AUTHOR INFORMATION

Corresponding Authors
*E-mail: sun@mie.utoronto.ca.
*E-mail: filleter@mie.utoronto.ca.
*E-mail: chandraveer.singh@utoronto.ca.

Author Contributions
§M.D. and C.C. contributed equally.

Notes
The authors declare no competing financial interest.

ACKNOWLEDGMENTS

REFERENCES

(1) Cai, D.; Song, M. A Simple Route to Enhance the Interface Between Graphite Oxide Nanoplatelets and a Semi-crystalline Polymer for Stress Transfer. *Nanotechnology* **2009**, *20*, 315708.

(2) Chen, S.; Zhu, J.; Wu, X.; Han, Q.; Wang, X. Graphene Oxide–MnO2 Nanocomposites for Supercapacitors. *ACS Nano* **2010**, *4*, 2822−30.

(3) Kim, M.; Lee, C.; Jang, J. Fabrication of Highly Flexible, Scalable, and High-Performance Supercapacitors Using Polyaniline/Reduced Graphene Oxide Film with Enhanced Electrical Conductivity and Crystallinity. *Adv. Funct. Mater.* **2014**, *24*, 2489−2499.

(4) Becerril, H. A.; Mao, J.; Liu, Z.; Stoltenberg, R. M.; Bao, Z.; Chen, Y. Evaluation of Solution-Processed Reduced Graphene Oxide Films as Transparent Conductors. *ACS Nano* **2008**, *2*, 463−70.

(5) Cao, C.; Daly, M.; Singh, C. V.; Sun, Y.; Filleter, T. High Strength Measurement of Monolayer Graphene Oxide. *Carbon* **2015**, *81*, 497−504.

(6) Dikin, D. A.; Stankovich, S.; Zimney, E. J.; Piner, R. D.; Dommett, G. H. B.; Evmenenko, G.; Nguyen, S. T.; Ruoff, R. S. Preparation and Characterization of Graphene Oxide Paper. *Nature* **2007**, *448*, 457−460.

(7) Gao, Y.; Liu, L.-Q.; Zu, S.-Z.; Peng, K.; Zhou, D.; Han, B.-H.; Zhang, Z. The Effect of Interlayer Adhesion on the Mechanical Behaviors of Macroscopic Graphene Oxide Papers. *ACS Nano* **2011**, *5*, 2134−2141.

(8) Wang, C.; Frogley, M. D.; Cinque, G.; Liu, L.-Q.; Barber, A. H. Deformation and Failure Mechanisms in Graphene Oxide Paper Using In Situ Nanomechanical Tensile Testing. *Carbon* **2013**, *63*, 471−477.

(9) Cao, C.; Daly, M.; Chen, B.; Howe, J. Y.; Singh, C. V.; Filleter, T.; Sun, Y. Strengthening in Graphene Oxide Nanosheets: Bridging the Gap between Interplanar and Intraplanar Fracture. *Nano Lett.* **2015**, *15*, 6528−6534.

(10) Peng, B.; Locascio, M.; Zapol, P.; Li, S.; Mielke, S. L.; Schatz, G. C.; Espinosa, H. D. Measurements of Near-Ultimate Strength for Multiwalled Carbon Nanotubes and Irradiation-Induced Crosslinking Improvements. *Nat. Nanotechnol.* **2008**, *3*, 626−631.

(11) Koziol, K.; Vilatela, J.; Moisala, A.; Motta, M.; Cunniff, P.; Sennett, M.; Windle, A. High-Performance Carbon Nanotube Fiber. *Science* **2007**, *318*, 1892−1895.

(12) Espinosa, H. D.; Filleter, T.; Naraghi, M. Multiscale Experimental Mechanics of Hierarchical Carbon-Based Materials. *Adv. Mater.* **2012**, *24*, 2805−2823.

(13) Soule, D. E.; Nezbeda, C. W. Direct Basal-Plane Shear in Single-Crystal Graphite. *J. Appl. Phys.* **1968**, *39*, 5122−5139.

(14) Bhushan, B.; Ling, X.; Jungen, A.; Hierold, C. Adhesion and Friction of a Multiwalled Carbon Nanotube Sliding against Single-Walled Carbon Nanotube. *Phys. Rev. B: Condens. Matter Mater. Phys.* **2008**, *77*, 165428.

(15) Yu, M.-F.; Yakobson, B. I.; Ruoff, R. S. Controlled Sliding and Pullout of Nested Shells in Individual Multiwalled Carbon Nanotubes. *J. Phys. Chem. B* **2000**, *104*, 8764−8767.

(16) Kis, A.; Jensen, K.; Aloni, S.; Mickelson, W.; Zettl, A. Interlayer Forces and Ultralow Sliding Friction in Multiwalled Carbon Nanotubes. *Phys. Rev. Lett.* **2006**, *97*, 025501.

(17) Koren, E.; Lortscher, E.; Rawlings, C.; Knoll, A. W.; Duerig, U. Adhesion and Friction in Mesoscopic Graphite Contacts. *Science* **2015**, *348*, 679−83.

(18) Blakslee, O. L.; Proctor, D. G.; Seldin, E. J.; Spence, G. B.; Weng, T. Elastic Constants of Compression-Annealed Pyrolytic Graphite. *J. Appl. Phys.* **1970**, *41*, 3373−3382.

(19) Wang, L.-F.; Ma, T.-B.; Hu, Y.-Z.; Wang, H. Atomic-Scale Friction in Graphene Oxide: An Interfacial Interaction Perspective from First-Principles Calculations. *Phys. Rev. B: Condens. Matter Mater. Phys.* **2012**, *86*, 125436.

(20) Lerf, A.; He, H.; Forster, M.; Klinowski, J. Structure of Graphite Oxide Revisited. *J. Phys. Chem. B* **1998**, *102*, 4477−4482.

(21) He, H.; Klinowski, J.; Forster, M.; Lerf, A. A New Structural Model for Graphite Oxide. *Chem. Phys. Lett.* **1998**, *287*, 53−56.

(22) Medhekar, N. V.; Ramasubramaniam, A.; Ruoff, R. S.; Shenoy, V. B. Hydrogen Bond Networks in Graphene Oxide Composite Paper: Structure and Mechanical Properties. *ACS Nano* **2010**, *4*, 2300−2306.

(23) Compton, O. C.; Cranford, S. W.; Putz, K. W.; An, Z.; Brinson, L. C.; Buehler, M. J.; Nguyen, S. T. Tuning the Mechanical Properties of Graphene Oxide Paper and Its Associated Polymer Nanocomposites by Controlling Cooperative Intersheet Hydrogen Bonding. *ACS Nano* **2012**, *6*, 2008−2019.

(24) Paci, J. T.; Belytschko, T.; Schatz, G. C. Computational Studies of the Structure, Behavior upon Heating and Mechanical Properties of Graphite Oxide. *J. Phys. Chem. C* **2007**, *111*, 18099−18111.

(25) Liu, Z.; Yang, J.; Grey, F.; Liu, J. Z.; Liu, Y.; Wang, Y.; Yang, Y.; Cheng, Y.; Zheng, Q. Observation of Microscale Superlubricity in Graphite. *Phys. Rev. Lett.* **2012**, *108*, 205503.

(26) Dienwiebel, M.; Verhoeven, G. S.; Pradeep, N.; Frenken, J. W. M.; Heimberg, J. A.; Zandbergen, H. W. Superlubricity of Graphite. *Phys. Rev. Lett.* **2004**, *92*, 126101.

(27) Hummers, W. S.; Offeman, R. E. Preparation of Graphitic Oxide. *J. Am. Chem. Soc.* **1958**, *80*, 1339−1339.

(28) Kudin, K. N.; Ozbas, B.; Schniepp, H. C.; Prud'homme, R. K.; Aksay, I. A.; Car, R. Raman Spectra of Graphite Oxide and Functionalized Graphene Sheets. *Nano Lett.* **2008**, *8*, 36−41.

(29) Chen, H.; Filleter, T. Effect of Structure on the Tribology of Ultrathin Graphene and Graphene Oxide Films. *Nanotechnology* **2015**, *26*, 135702.

(30) Wang, J.; Liang, M.; Fang, Y.; Qiu, T.; Zhang, J.; Zhi, L. Rod-Coating: Towards Large-Area Fabrication of Uniform Reduced Graphene Oxide Films for Flexible Touch Screens. *Adv. Mater.* **2012**, *24* (21), 2874−2878.

(31) Maugis, D. Adhesion of Spheres: the JKR-DMT Transition Using a Dugdale Model. *J. Colloid Interface Sci.* **1992**, *150*, 243−269.

(32) Carpick, R. W.; Ogletree, D. F.; Salmeron, M. A General Equation for Fitting Contact Area and Friction vs Load Measurements. *J. Colloid Interface Sci.* **1999**, *211*, 395−400.

(33) Kim, S.; Zhou, S.; Hu, Y.; Acik, M.; Chabal, Y. J.; Berger, C.; de Heer, W.; Bongiorno, A.; Riedo, E. Room-Temperature Metastability of Multilayer Graphene Oxide Films. *Nat. Mater.* **2012**, *11*, 544−549.

(34) Suk, J. W.; Piner, R. D.; An, J.; Ruoff, R. S. Mechanical Properties of Monolayer Graphene Oxide. *ACS Nano* **2010**, *4*, 6557−6564.

(35) Erickson, K.; Erni, R.; Lee, Z.; Alem, N.; Gannett, W.; Zettl, A. Determination of the Local Chemical Structure of Graphene Oxide and Reduced Graphene Oxide. *Adv. Mater.* **2010**, *22*, 4467−4472.

(36) Carlsson, J. M.; Ghiringhelli, L. M.; Fasolino, A. Theory and Hierarchical Calculations of the Structure and Energetics of [0001] Tilt Grain Boundaries in Graphene. *Phys. Rev. B: Condens. Matter Mater. Phys.* **2011**, *84*, 165423.

(37) Cannara, R. J.; Eglin, M.; Carpick, R. W. Lateral Force Calibration in Atomic Force Microscopy: A New Lateral Force Calibration Method and General Guidelines for Optimization. *Rev. Sci. Instrum.* **2006**, *77*, 053701.

(38) Sader, J. E.; Chon, J. W. M.; Mulvaney, P. Calibration of Rectangular Atomic Force Microscope Cantilevers. *Rev. Sci. Instrum.* **1999**, *70*, 3967−3969.

(39) Plimpton, S. Fast Parallel Algorithms for Short-Range Molecular Dynamics. *J. Comput. Phys.* **1995**, *117*, 1−19.

(40) Van Duin, A. C. T.; Dasgupta, S.; Lorant, F.; Goddard, W. A. ReaxFF: A Reactive Force Field for Hydrocarbons. *J. Phys. Chem. A* **2001**, *105*, 9396−9409.

(41) Jeong, H.-K.; Lee, Y. P.; Lahaye, R. J. W. E.; Park, M.-H.; An, K. H.; Kim, I. J.; Yang, C.-W.; Park, C. Y.; Ruoff, R. S.; Lee, Y. H. Evidence of Graphitic AB Stacking Order of Graphite Oxides. *J. Am. Chem. Soc.* **2008**, *130*, 1362−1366.

(42) Stukowski, A. Visualization and Analysis of Atomistic Simulation Data with OVITO−the Open Visualization Tool. *Modell. Simul. Mater. Sci. Eng.* **2010**, *18*, 015012.